



INVESTIGATION OF CHARACTERIZATION, MAGNETIC AND ANTI BACTERIAL PROPERTIES OF NICKEL DOPED WITH MANGANESE/COPPER NANOPARTICLES PREPARED BY SOL-GEL METHOD

A. Victor Bastin*, Meenakshi Sundar

Department of Physics, Sri Paramakalyani College Affiliated to Manonmaniam Sundaranar University, Alwarkurichi, Tirunelveli, Tamilnadu, India.

*Corresponding author: victorbastin19@gmail.com

ABSTRACT

The aim to study the effect of Nickel on structural, morphological, magnetic, antibacterial and antioxidant properties of sol gel derived manganese copper nanoparticles by sol gel technique with systematic investigation have been carried out. Manganese acetate dehydrate, copper acetate and nickel acetate tetra hydrate are used as the precursor material and dopant, respectively. The XRD pattern contained sharp peaks of Ni-manganese copper nanoparticles with mixed cuprite and tenorite phases. The morphologies of manganese copper nanoparticles were influenced by doping with Ni, as shown from the SEM images. The hysteresis loops of those Ni doped nanoparticles analogues displayed extremely magnetic scenery of those nanoparticles at room temperature which once saturation magnetization, coercivity and remanence magnetization reduced lineally over the increase in Ni-concentration in manganese copper nanoparticles. Pathogenic bacteria, such as *Escherichia coli*, *S. Haemolyticus*, *Aeromonas hydrophila*, *Cronobacter sakazakii*, *Aeromonas salmonicida* and *Basillus subti* were used to assess the antibacterial activity of the synthesized materials. The reduction in the viability of all the bacteria to zero using Ni-doped manganese copper nanoparticles occurred and it plays a vital role in the increased antibacterial activity performance. Here we concluded that the M_4 is promising candidate for medicinal application because of higher magnetic properties, antibacterial and antioxidant activity compared to other samples.

Keywords: Nanoparticles, Manganese, Copper, Antioxidant, Magnetic

1. INTRODUCTION

Nanostructured materials have attracted enormous interest due to their novel physical and chemical properties and promising applications in nano devices [1]. Nanostructure metal oxides have been actively studied for both scientific interest and potential applications [2]. The metal oxides can adopt a large variety of structural geometries with an electronic structure that may exhibit metallic, semiconductor or insulator characteristics endowing with their chemical and physical properties [3]. Recently, oxide based diluted magnetic semiconductors (DMS) such as transition metal doped semiconductors with room temperature ferromagnetism (RTFM) have been studied for advanced applications in spintronic devices where the effort was made to find the ways for the utilization of nanoparticles in both information processing and data storage within one material system. In recent studies, DMSs are formed by the potential substitution of the cations of the host semiconductors with small amount of transition metal (TM) ions [4]. TM

doped semiconductors have attracted a lot of attention due to their important applications such as UV detectors, field-effect transistors, short wavelength lasers, high sensitive chemical sensors and nonlinear varistors [5-7]. Several researchers addressed room temperature (RT) ferromagnetic behavior of 3d transition metals (such as Fe, Mn, Ni, Co, Cr etc.) doped semiconductor oxides [8-10]. Among the magnetic-metals, Ni is an important dopant to achieve Curie temperature (T_c) above the room temperature. Some reports revealed that the ferromagnetism (FM) of Ni doped ZnO NPs at 2K, while the material exhibited super paramagnetic behavior above 30K. Some research groups observed paramagnetic and FM nature in ZnO at RT with different Ni content [11]. A variety of chemical techniques were used to synthesize nanomaterials, such as solvothermal [12], hydrothermal [13], co-precipitation [14] and sol-gel methods [15], etc. Among these synthetic routes, co-precipitation method has been popularly adopted to synthesis NPs due to its

low cost and high yield of nanoparticles with uniform size.

Copper nanoparticles have gained as the most attractive nanoparticles in the field of multidisciplinary science [16]. Typically, copper nanoparticles are synthesized using several chemical and physical approaches based on the appropriateness of the methods to achieve the desirable applications [17]. Physical methods used for the synthesis of copper nanoparticles implicate expensive instruments and sophisticated techniques. While, using chemical approaches copper nanoparticles are synthesized by several chemical reductants such as trisodium citrate, sodium borohydride, hydrazine [18]. Even though chemical approaches have been extensively applied for the synthesis of copper nanoparticles but the precarious reductants and several organic solvents used for the synthesis are potentially hazardous for the environment [19]. Therefore, the development of affordable solutions is in demand to efficiently reduce the hazardous risks of chemical reductants [20].

In addition, copper nanoparticles have attained great interests due to their distinctive physicochemical properties that make them effective agents against different classes of pollutants. Due to differentiated properties, copper nanoparticles exhibits sorbent properties that directly used for the elimination of toxic inorganic metal pollutants and organic dyes from industrialized wastewater [21]. The copper nanoparticles are broadly used as antibacterial agents because of low toxicity and biodegradable nature [22]. These copper nanoparticles also exhibit the mechanism of antibacterial properties due to their large surface area relative to the volume that proficiently decreases the oxygen stream by binding with the cell wall that ultimately causes the reduction in respiration. According to previous research there is no other research about manganese copper doped with silver for magnetic performance. In this study is we report structural, antibacterial, antioxidant and magnetic properties of manganese copper nanoparticles doped with silver nanoparticles synthesized from manganese acetate, copper acetate and Nickel acetate by using sol gel method.

2. MATERIAL AND METHODS

2.1. Chemicals

All the chemicals are of analytical grade and used without further purification. Manganese (II) acetate, Copper acetate, and Nickel acetate (5%), DD water and aluminum foil (0.025 mm thickness) were purchased

from Alfa Aesar. The solutions are freshly prepared using Millipore water.

2.2. Nanoparticles synthesis

The Mn/Cu nanoparticles were prepared by the sol-gel technology. Reagent grade chemicals were used without further purification. The calculated amounts of Manganese acetate, copper acetate and silver acetate were mixed in 2 mol L⁻¹ nitric acid by stirring for 1 h at pH~4-5, followed by addition of 30 mL of 1.5 mol L⁻¹ citric acid solutions. The resulting solution turned to yellowish sol then the sol was stirred continuously using a magnetic stirrer at 60°C until it became a transparent sticky gel. At that point, the gel was dried in an air oven at 200°C for 1 h which leads the formation of light weight porous materials due to the enormous gas evolution, and it was sintered at 850°C for 4 h to get the fine homogeneous dense powder. According to our previous study proved better characterization and properties which is manganese acetate (0.5%) with copper acetate (0.5%) doped with silver. Nickel acetate (0.2%, 0.4%, 0.6% 0.8 and 1% named as M₁, M₂, M₃, M₄ and M₅ respectively) was mixed gently with 0.5mL deionized water (DI) add to manganese acetate (0.5%) with copper acetate (0.5%). After gelation, the NPs were left to dry at 100°C for 24 hours.

2.3. Structural characterization

The crystallinity of the prepared nanoparticles was studied by XRD pattern with the help of X'Pert PRO PANalytical X-ray diffractometer. FTIR spectroscopic technique is a nondestructive technique. FTIR spectra were recorded using the Thermo Nicolet instrument in the wave number in the range of 400- 4000 cm⁻¹ were scanned over a range of 20-80°. SEM (JEOL JSM-5610 analysis station SEM) was utilized to examine the shape and cross-sectional morphology of synthesized silver doped nanoparticles. The UV-Vis diffuse reflectance spectra were measured using a PerkinElmer Lambda 35 spectrometer which was operated at a wavelength range of 200-800 nm. At last the aim to analyze the attractive properties, VSM (Lake Shore display 7407) examination was utilized at a room temperature with greatest connected attractive field of 15 kG.

2.4. Antibacterial Activity of Nanoparticles

Bacterial strains including *Escherichia coli*, *S.aureus*, *Aeromonas hydrophila*, *Cronobacter sakazakii*, *Aeromonas salmonicida* and *Basillus subtilis* were used for experiment.

50ml of LB broth was prepared in 250ml conical flask and the bacterial strains were grown in this medium at 37°C on an orbital shaker. The culture flask was inoculated at 0.1 OD 600nm with freshly prepared LB medium under same culture conditions. The mid log phase bacterial cultures were used for the antibacterial studies. 0.1 OD of overnight different bacterial cultures was swabbed on the 25ml LB agar plates. Then the whatman disk was placed on the plates. About 30ul of Mn/Cu/Ni nanoparticles (M₁, M₂, M₃, M₄ and M₅) samples were add on that whatman disc and incubate for overnight at 37°C.

2.5. DPPH Assay

The DPPH scavenging assay of M₁, M₂, M₃, M₄ and M₅ was evaluated after the Rejiniemon et al., 2015 [23]. First we prepared 0.15% DPPH in ice cold methanol. The reaction mixture contains 3.8 ml of methanol add various concentration of M₁, M₂, M₃, M₄ and M₅ and then add 200 µL of DPPH solution then it make incubated at normal temperature for 30min in dark condition. After incubation time the absorbance have make the process at 517nm. Vitamin C has a use of a standard. The DPPH radical scavenging activity was calculated using the given equation:

DPPH radical scavenging activity (%) = $[(A_0 - A_1 / A_0) * 100]$, where A₀ is the absorbance of the rule at 30 min and A₁ is the absorbance of the paradigm at 30 min. All paradigms have examined in triplicate.

2.6. Hydrogen Peroxide Scavenging Activity

Ethyl acetate extract of M₁, M₂, M₃, M₄ and M₅ of hydrogen peroxide activity was evaluated after the Frank Ngonda 2013 method [24]. 40mm of H₂O₂ was taken in phosphate buffer ph 7.4. The reaction mixtures contains various concentration of M₁, M₂, M₃, M₄ and M₅ and add 1ml of distilled water then add 0.6ml of H₂O₂ incubated for 10 min at normal temperature. According to incubation the absorbance was adopted at 560nm. The ascorbic acid was used as a standard. The hydrogen peroxide scavenging activity of M₁, M₂, M₃, M₄ and M₅ was calculated by the equation:

Hydrogen peroxide radical scavenging activity (%) = $[(A_0 - A_1 / A_0) * 100]$, where A₀ is the absorbance of the rule at 10 min and A₁ is the absorbance of the paradigm at 10 min. All paradigms are termed in triplicate.

2.7. Superoxide radical scavenging activity

Superoxide scavenging activity of M₁, M₂, M₃, M₄ and M₅ was measured using NBT according to Sunil et al., [25]. Nitrate reduction occurs during generation of superoxide radicals by oxidation of hydroxyl amine hydrochloride in the presence of NBT (Nitro blue tetrazolium). Test solutions of the M₁, M₂, M₃, M₄ and M₅ (20-100 µL) were taken in a test tube. To this, add 1 mL water, 100 µL of (24 mM) NBT, and 0.2 mL of 0.1 mM EDTA solutions was added to the test tube. About 0.1 mL of (1 mM) of hydroxylamine hydrochloride was added to initiate the reaction; then reaction mixture was incubated at 25°C for 15 min and reduction of NBT was measured at 560 nm and without extract used as a control:

Superoxide radical scavenging activity (%) = $[(A_0 - A_1 / A_0) * 100]$, where A₀ is the absorbance of the control at 15 min and A₁ is the absorbance of the sample at 15 min. All samples were analyzed in triplicate.

2.8. Hydroxyl radical scavenging activity

The hydroxyl scavenging assay of M₁, M₂, M₃, M₄ and M₅ was performed as described by the method of Sunil et al. [25]. All solutions were prepared freshly. The reaction mixture contained 100 µL of 28 mM 2-deoxy-2-ribose (dissolved in phosphate buffer, pH 7.4), add different volume of M₁, M₂, M₃, M₄ and M₅ (20-100 µL) and then mixed with 1ml of distilled water, 200 µL of 100 mM FeCl₃ and 100 mM EDTA (1:1 v/v), 100 µL H₂O₂ (1 mM), and 100 µL ascorbic acid (1 mM). After an incubation period of 1 h at 37°C, the extent of deoxyribose degradation was measured by the TBA reaction. The absorbance was read at 532 nm against the blank solution. Vitamin C was used as a positive control and without extract used as a control. The scavenging activity was calculated by formula:

Hydroxyl radical scavenging activity (%) = $[(A_0 - A_1 / A_0) * 100]$, where A₀ is the absorbance of the control at 1 hour and A₁ is the absorbance of the sample at 1 hour. All samples were analyzed in triplicate.

3. RESULTS AND DISCUSSION

3.1. X-ray diffraction analysis

The XRD pattern of Ni-doped Mn/Cu nanoparticles samples is shown in Figure 1. To evaluate the crystalline structures M₁, M₂, M₃, M₄ and M₅ prepared nanoparticles. From the figure 1 shows that the four

major crystalline planes are identified at $2\theta=39.87^\circ$, 43.3° , 50.5° and 77.9° corresponds to the XRD pattern of synthesized nanoparticles. These crystalline peaks well matched to the (211), (111), (200) and (311) planes. The XRD peaks of manganese phases for the sample containing copper are considerably wider. The peaks at $2\theta = 34$ degrees assigned in tetragonal $K2-xMn_8O_{16}$ to (110) reflection lines, are no longer visible on the XRD curve of Mn/Cu sample and only wide singular peak is detectable. Similarly, the peak located at $2\theta = 43.3$ (the reflection line (111)) is much higher. Small peaks located at 50.5 and 77.9 degrees are almost undetectable. Such effects can be related to the presence of very small cryptomelane nanoparticles and may also indicate the formation of manganese oxides of different crystallographic structures. It is worth noting that neither separated peaks of copper-manganese nor copper oxide phases, in spite of the relatively large amount of Cu are not observed. This reveals a strong dispersion of manganese and copper species [26, 27]. This is evidenced by the presence of Ni in the diffractogram of the Ag-doped samples with the relative intensity of the stronger Ni peaks, (020) at 2θ of 28.08° . Furthermore, the intensity of the peaks increased with increasing the concentration of Ni. This result agrees with that of other reports [28], in which calcinations is used to increase the crystallinity of Mn/Cu nanoparticles by decreasing the e^-h^+ pair recombination and enhance the antibacterial activity as well.

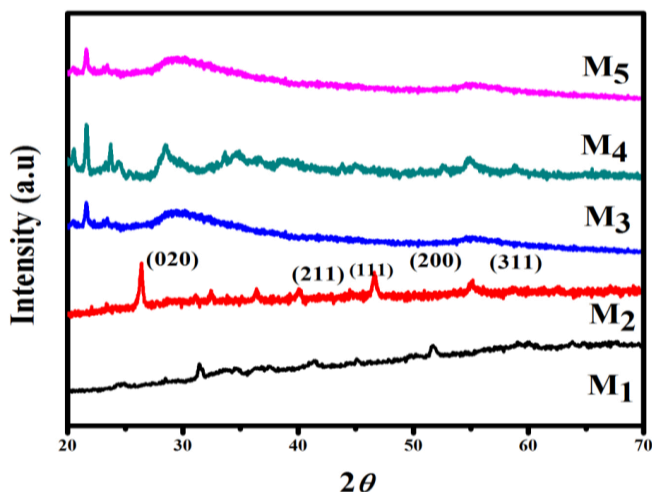


Fig. 1: XRD patterns of silver doped manganese copper nanoparticles M_1 , M_2 , M_3 , M_4 and M_5

3.2. FTIR analysis

The FTIR spectra of Nickel doped manganese and copper nanoparticles M_1 , M_2 , M_3 , M_4 and M_5 were recorded in

the range of $400-4000\text{cm}^{-1}$ are shown in figure 2. The weak absorption peaks observed at 3200cm^{-1} and 3500cm^{-1} may be attributed to alkynes groups. The fundamental absorption peaks at 1566cm^{-1} and 1041cm^{-1} are assigned to the bending and stretching vibrations of O-H groups [29]. The changes in the frequencies are associated with the coordination of nanoparticles with amino groups, and these are more evident in the vibrations of N-H and C-N bonds.

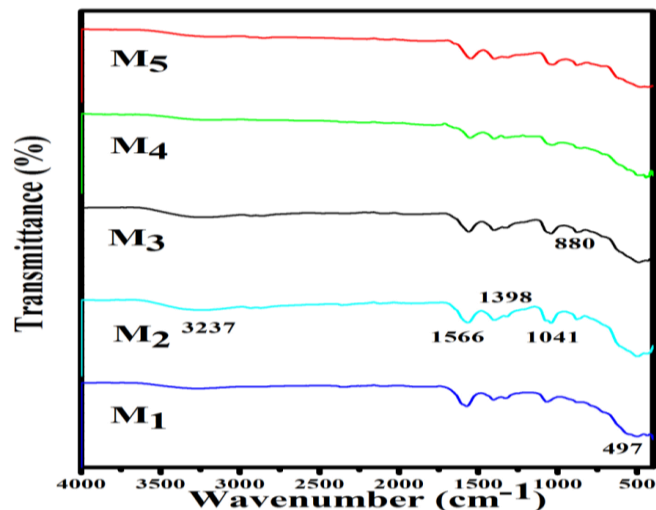


Fig. 2: FTIR analysis of silver doped manganese copper nanoparticles M_1 , M_2 , M_3 , M_4 and M_5

3.3. Optical Properties

As shown in Figure 3, M_1 , M_2 , M_3 , M_4 and M_5 exhibited atypical absorption characteristics due to a band gap change in the range $350-370\text{nm}$ in the visible region caused by the surface plasmon band characteristics of Nickel; it was further confirmed that Ni was effectively deposited on the surface of Mn/Cu nanoparticles [30].

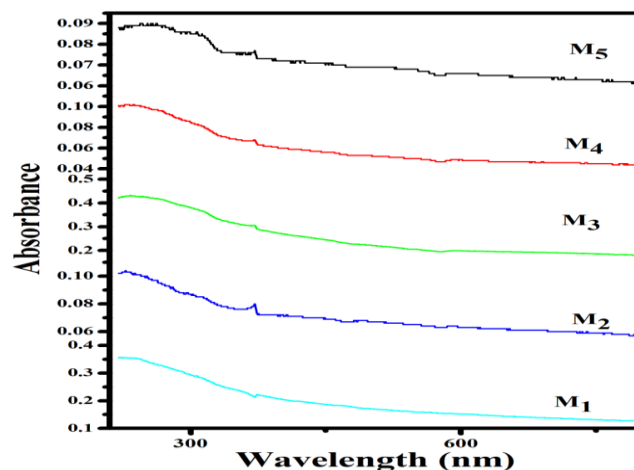


Fig. 3: UV absorptions of silver doped manganese copper nanoparticles M_1 , M_2 , M_3 , M_4 and M_5

The shift in absorption spectra provides some evidence of the interaction between Ni and Mn/Cu nanoparticles, which is also in agreement with the XRD patterns.

3.4. SEM analysis

The morphologies of M_1 , M_2 , M_3 , M_4 and M_5 nanoparticles were observed by SEM. The morphology of M_1 , M_2 , M_3 , M_4 and M_5 nanoparticles was examined by SEM (Fig. 4). It was apparent from the SEM image that the tenorite particles were spherical in shape and that interconnection of a multigranular structure led to greater porosity than for cuprite, which was in the form

of pyramid aggregates which resulted in a compact material. Figures show the morphologies of the samples and Ni distribution in the as synthesized samples. It can be seen that the surface of Ni in Figures is smooth. Similar surface morphology of copper oxide nanoparticles has also been reported in the literature [31-33] Nanoparticles agglomerated during increasing the concentration of Ni. Comparison of the morphology of nanoparticles M_1 , M_2 , M_3 , M_4 and M_5 revealed that the shape of Ni doped Mn/Cu nanoparticles nanostructures could be modified by changing the concentration of dopant.

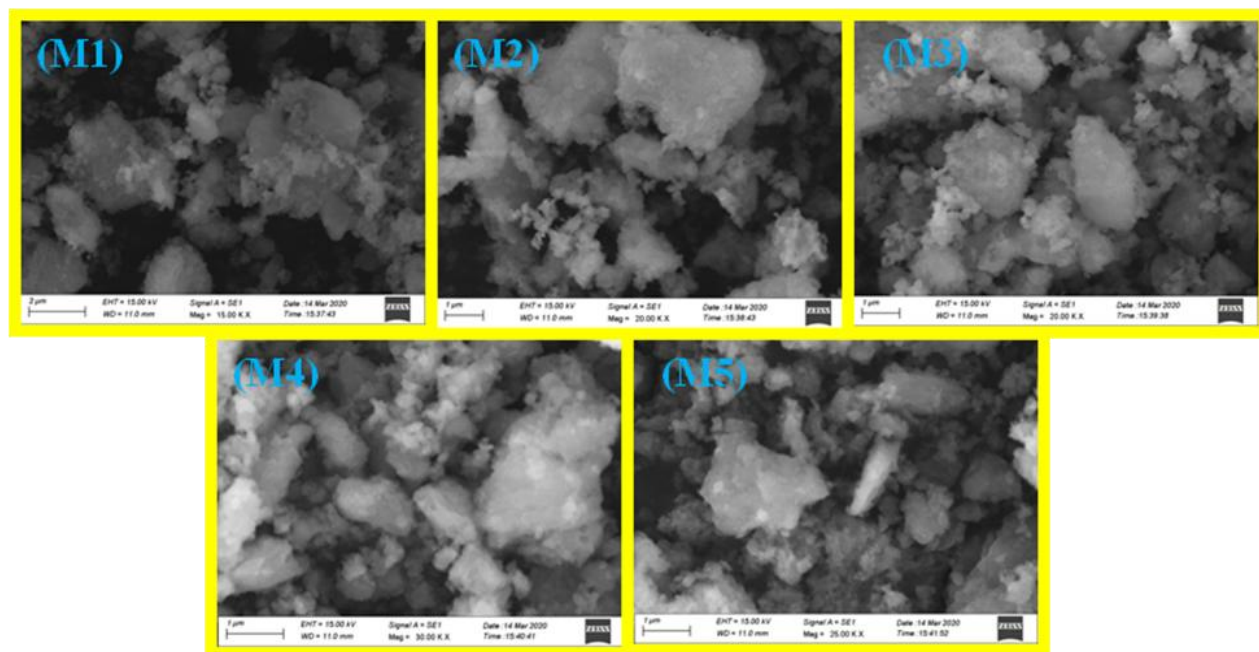


Fig. 4: SEM images of silver doped manganese copper nanoparticles M_1 , M_2 , M_3 , M_4 and M_5

3.5. Magnetic measurements

Magnetization estimations were taken out on those models at room temperature utilizing investigates coil technique. Fig. 5 displays the hysteresis loops for each and every one of the models showing the coercivity (HC), saturation magnetization (MS) and remanence magnetization (Mr) for all models. As seen from M-H loops of M_1 , M_2 , M_3 , M_4 and M_5 models, coercivity of the models reduced with raising x values. This is owing to lesser magneto crystalline anisotropy of Ni^{2+} as far that of Mn/Cu^{2+} [34]. Figure displays that Ms Value of the models reduced as the Ni content increases. An equivalent pattern of reduced in saturation magnetization with Ni^{2+} ion substitution in Mn/Cu^{2+} had been recorded [35, 36]. This decline in Ms with expanding nickel substance is ascribed to the smaller magnetic moment of

Ni^{2+} (2 #B) when contrasted with higher magnetic moments of Mn/Cu^{2+} (3 #B) consistently similarly conveyed among tetrahedral and octahedral sites which obtained a net magnetic moment of 2 #B per equation unit for Ni doped Mn/Cu nanoparticles and 3 #B per equation unit for Mn/Cu. Therefore, the expansion in Ni content inside the host lattice leads to the reduction in Ms Values. This occurrence might be ascribed to two reasons: (1) the synthesized particles are sufficient to give the domain walls, and the coercivity (Hc) of nanoparticles should be decreased by magnetization turn around over the domain wall [37]; (2) with the increasing x value, the magnetic anisotropy decreases, most important to the simpler inversion of minutes with a lower Hc esteem. Subsequently, the abatement of Ms owes at a bit of magnetic moment of nickel as associated

for cobalt [38]. This is further same because of inert or dead layer at the surface (shell) of nanoparticles that protect the core ferromagnetic spins to align with the field direction. As a conclusion the immersion charge in the event of nanoparticles reduced. Further purpose behind the diminished magnetization in nanoparticles is the inclined twists or turn glass like layer at the outside of the nanoparticles that enlarge due to the widely division of surface to volume molecules in little particles. These canted spins usually decreased the saturation magnetization in those nanoparticles. Inferable from this impact (canted spins) at the surface (shell) of nanoparticles, no true saturation in those particles is succeeded even at exceptionally high connected field involved the decreasing of magnetization in the smaller particles.

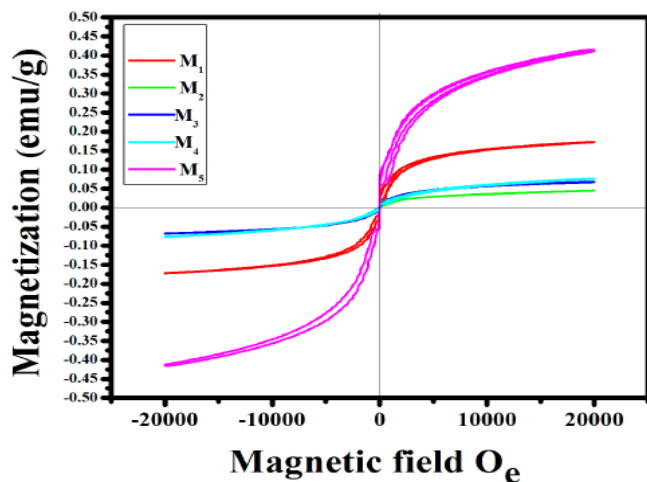


Fig. 5: M-H loops of the M_1 , M_2 , M_3 , M_4 and M_5 nanoparticles

3.6. Antibacterial activity

Interestingly, Ni doped M_1 , M_2 , M_3 , M_4 and M_5 nanoparticles are a promising candidate which shows an excellent antibacterial activity against all bacteria. In this present work antibacterial activity of Ni doped M_1 , M_2 , M_3 , M_4 and M_5 nanoparticles against bacterial strains *Escherichia coli*, *S. Haemolyticus*, *S.aureus*, *Cronobacter sakazakii*, *Aeromonas salmonicida* and *Basillus subtilis* were investigated by the disc diffusion agar method. From the figure it is evident that Ni doped M_1 , M_2 , M_3 , M_4 and M_5 nanoparticles showed activity towards all pathogens. From the figure 6 it is found that zone of inhibition was increased with increasing concentration Ni content till 0.8% and then it was decreased, which may be due to the reason that the particle size is lower in case of doped nanoparticles. This implies that the particle size is one of the key factors to influence the antibacterial activity.

Sourav Das et al. 2017 [39] stated the similar results of antibacterial activity against *Escherichia coli* by Solar-Photocatalysis using Fe-doped ZnO. Jones et al. [40] tried to identify the potential antibacterial effect of ZnO nano structure against both Gram-positive (*S.aureus*, *Bacillus subtilis*) and Gram-negative (*E.coli*) microorganisms. In comparison with these results mentioned above, our results showed better growth of inhibition against both bacteria.

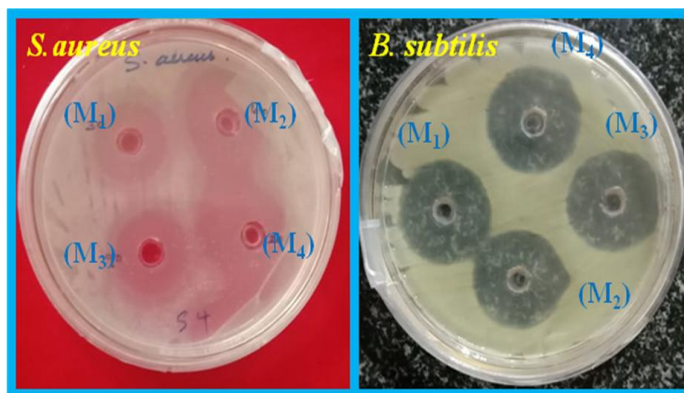


Fig. 6: Antibacterial activity of Ag doped M_1 , M_2 , M_3 , M_4 and M_5 nanoparticles

3.7. DPPH Assay

DPPH radical scavenging movement is the basic efficient methods for screening the antioxidant activity of Ni doped M_1 , M_2 , M_3 , M_4 and M_5 nanoparticles. The outcome of DPPH free radical scavenging activity of Ni doped M_1 , M_2 , M_3 , M_4 and M_5 nanoparticles are viewed in figure 7.

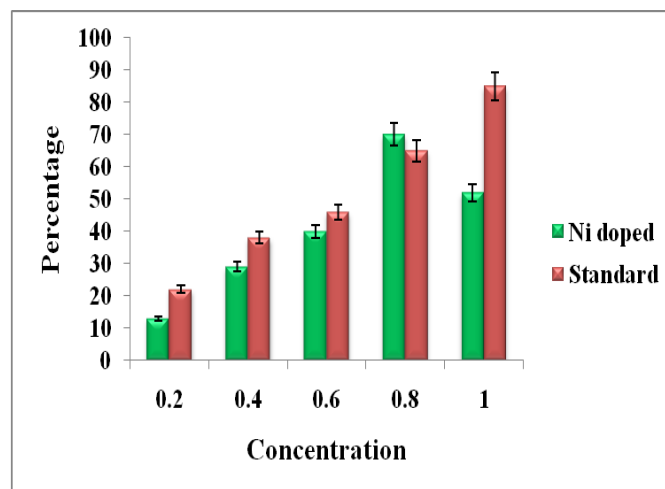


Fig. 7: DPPH Assay of nanoparticles

From the outcome they show the comparatively active against standard ascorbic acid. Ni doped M_1 , M_2 , M_3 , M_4

and M_5 nanoparticles having activity depend on concentration manner. Ni doped nanoparticles 19.2% DPPH activity showed at 0.2% and 76.88% at 0.8% Ni content and after that it decreased; the 1% of Ni content was showed 63%.

3.8. Hydrogen Peroxide Radical Scavenging Activity

Hydrogen peroxide can cross cell membranes promptly, once inside the cell, H_2O_2 can apparently respond with Fe^{2+} , and conceivably Cu^{2+} ions to form hydroxyl radical with this might be the root of a larger number of its toxic effects. The hydrogen peroxide radical scavenging activity demonstrated relies upon the grouping of Ni doped M_1 , M_2 , M_3 , M_4 and M_5 nanoparticles. The increased concentration increased scavenging activity and the outcome is seen in figure 8. The hydrogen peroxide radical scavenging activity showed highest activity in 74.73% at 0.8% Ni doped M_4 nanoparticles and in 60.07% at 1%. Hydrogen peroxide activity showed more activity 74.73 ± 2.7 at 0.8% Ni doped M_4 .

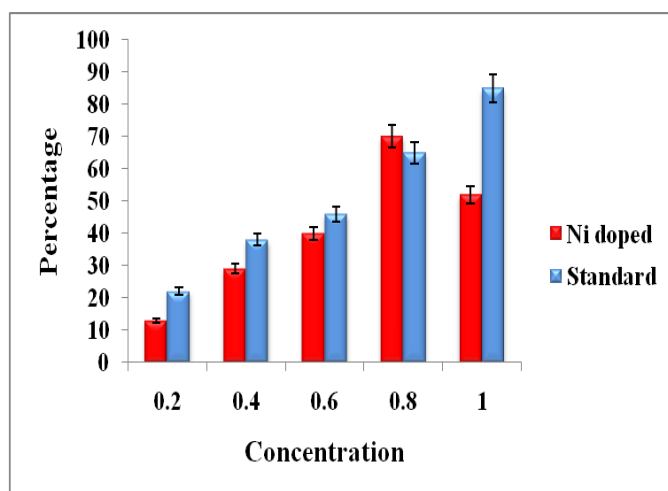


Fig. 8: Hydrogen Peroxide Radical Scavenging Activity of nanoparticles

3.9. Superoxide radical scavenging activity

Superoxide radical scavenging activity was measured using M_1 , M_2 , M_3 , M_4 and M_5 by the inhibition of percentage of superoxide radical generation and compared with vitamin C. This activity results showed in comparison manner with standard ascorbic acid. About 50% of superoxide radical scavenging activity showed in $80 \mu\text{L/ml}$. Highest activity showed 54.1% for M_4 and standard ascorbic acid showed highest activity in 79.67% at $100 \mu\text{L/ml}$. Superoxide radical scavenging activity of M_1 , M_2 , M_3 , M_4 and M_5 are shown in figure 9.

Superoxide radical scavenging activity showed more activity 54.1 ± 0.7 at M_4 .

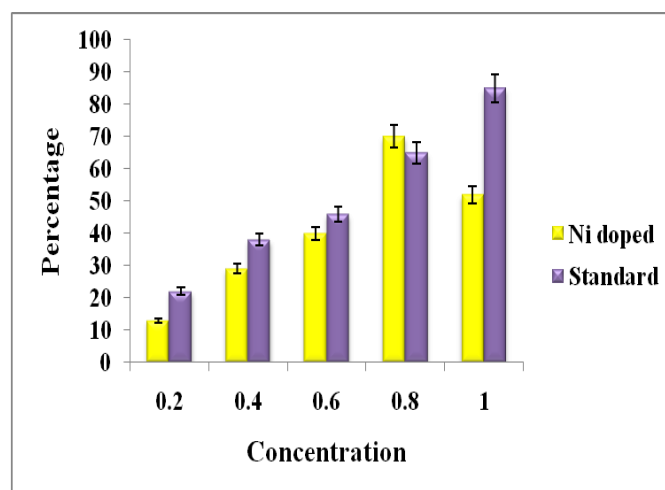


Fig.9: Superoxide radical scavenging activity of nanoparticles

3.10. Hydroxyl radical scavenging activity

The hydroxyl radical is a particularly reactive in biological systems and has been associated with as highly damaging species in free radical pathology, competent of damaging bimolecular of the living cells. These radical combines with nucleotides in DNA and cause strand breakage leading to carcinogenesis, mutagenesis and cytotoxicity. Hydroxyl radical ($\bullet\text{OH}$) scavenging capacity of an extract is directly related to its antioxidant activity. The hydroxyl radical scavenging activity showed highest activity in 70.9 % at M_4 and standard ascorbic acid showed in 72.09% at $100 \mu\text{L/ml}$. Hydroxyl radical scavenging activity showed more activity 70.9 ± 0.4 at M_4 and results were showed in figure 10.

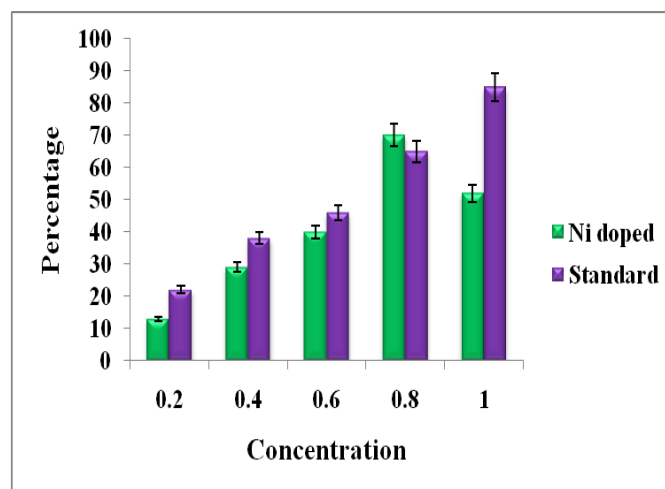


Fig.10: Hydroxyl radical scavenging activity of nanoparticles

4. CONCLUSION

In conclusion, we synthesized Nickel doped manganese copper nanoparticles for enhanced structural morphological, magnetic, antimicrobial and antioxidant efficacy using sol-gel method. Based upon particle size, nickel doped manganese copper nanoparticles capped with 0.8% nickel were found to be the most suitable nanoparticles for enhanced magnetic, antimicrobial and antioxidant efficiency. In addition, manganese copper nanoparticles capped with nickel were highly oxidative stable and they could be directly used as additives for antibacterial formulation. As well, nanoparticles could be used for the purification of waste-water.

5. REFERENCES

- Cui YF, Wang C, Wu SJ, Liu G, Zhang FF, Wang TM. *Cryst. Eng. Comm.*, 2011; **13**:4930-4934.
- Masoud Salavati-Niasari, Afsaneh Khansari, Fatemeh Davar, *Inorg. Chim. Acta*, 2009; **362**:4937-4942.
- Ball P, Garwin L. *Nature*, 1992; **355**:761-766.
- Guangqing Pei M, Changtai X, Bo W, Tao W, Lili Z, Yongjun D, Jun X. *Comput. Mater. Sci.*, 2008; **43**:489-494.
- Johnson JC, Yan H, Yang P, Saykally RJ. *J. Phys. Chem. B*, 2003; **107**:8816-8828.
- Fan Z, Lu JG. *Appl. Phys. Lett.*, 2005; **86**:123510.
- Ng HT, Han J, Yamada T, Nguyen P, Chen YP, Meyyappan M. *Nano Lett.*, 2004; **7**:1247-1252.
- Radovanovic PV, Gamelin DR. *Phys. Rev. Lett.*, 2003; **91**: 157202.
- Norberg NS, Kittilstved KR, Amonette JE, Kukkadapu RK, Schwartz DA, Gamelin DR. *J. Am. Chem. Soc.*, (2004) **126**:9387-9388.
- Ueda K, Tabata H, Kawai T. *Appl. Phys. Lett.*, 2001; **79**:988-990.
- Xai C, Hu C, Tian Y, Wan B, Xu J, He X. *Physica E*, 2010; **42**:2086-2090.
- Liu Z, Zhang Q, Shi G, Li Y, Wang H. *J. Magn. Magn. Mater.*, 2011; **323**:1022-1026.
- Gao S, Li V, Lv X, Wang J, Li H, Yu Q, Guo F, Zhao L. *J. Alloys Comp.*, 2012; **539**:200-204.
- Vijayaprasath G, Ravi G, Haja Hameed AS, Mahalingam T. *J. Phys. Chem., C*, 2014; **118**:9715 - 9725.
- Arshad M, Azama A, Ahmed AS, Mollah S, Naqvi AH. *J. Alloys Comp.*, 2011; **509**:8378-8381.
- Tiwari M, Jain P, Hariharapura RC, Narayanan K, Bhat U, Udupa N, Rao JV. *Process Biochem.* 2016; **51(10)**:1348-1356.
- Suárez-Cerda J, Espinoza-Gómez H, Alonso-Núñez G, Rivero IA, Gochi- Ponce Y, Flores-López LZ. *J Saudi Chem Society.*, 2017; **21(3)**:341- 348.
- Nagar N, Devra V. *Materials ChemPhy.*, 2018; **213**:44-51.
- Rajendaran K, Muthuramalingam R, Ayyadurai S. *Mat SciSemicon Proc.* 2019; **91**:230-238.
- Fathima JB, Pugazhendhi A, Oves M, Venis R. *J Molliq*, 2018; **260**:1-8.
- Sebeia N, Jabli M, Ghith A. *InorgChemCommun.* 2019; **105**:36-46.
- Jain S, Bhanjana G, Heydarifard S, Dilbaghi N, Nazhad MM, Kumar V. *Carbohydrate polymers*, 2018; **202**:219-226.
- Naif Abdullah Al-Dhabi, Mariadhas Valan Arasu, and Thankappan Sarasam Rejiniemon. *Evidence-Based Complementary and Alternative Medicine*, 2015; <https://doi.org/10.1155/2015/164261>.
- Frank Ngonda. *Asian Journal of Biomedical and Pharmaceutical Sciences*; 2013; **3(20)**:21-25.
- Sunil C, Irudayaraj SS, Duraipandiyar V, Al-Dhabi NA, Agastian P, and Ignacimuthu S. *Industrial Crops and Products*, 2014; **61**:510-516.
- Cheng B, Le Y, and Yu J. *Journal of Hazardous Materials*, 2010; **177**, 1–3:971-977.
- Gupta K, Singh RP, Pandey A, Pandey A. *Beilstein Journal of Nanotechnology*, 2013; **4**:345-351.
- Darezereszki E and Bakhtiari F. *J. Min. Metall. Sect. B.*, 2011; **47**:73.
- Maccato C, Simon Q, Carraro G, Barreca D, Gasparotto A, Lebedev OI, Turner S, Tendeloo GV. *J. Adv. Microsc. Res.*, 2012; **7**:84.
- Kumaresan K, Ramamurthi N, Mathuri S, Sinthiya MMA, Manimozhi T, Margoni MM, and Rameshbabu V. *Int. J. Chem. Tech Res.* 2015; **7**:1598.
- Kefeni KK, Mamba BB, Msagati TA. *Sep. Purif. Technol.*, 2017; **188**:399-422.
- Nikmanesh H, Eshraghi M, Karimi S. *Journal of Magnetism and Magnetic Materials.*, 2018; **09**:102.
- Panda RK, Muduli V, Behera D. *J. Alloy. Compd.* 2015; **634**:239.
- Toksha BG, Sagar, Shirsath ML, Mane SM, Patange SS, Jadhav KM E. *J. Phys. Chem. C*, 2011; **115**:20905.
- Kriebel K, Lo CCH, Melikhov Y, Snyder JE. *J. Appl. Phys.*, 2006; **99**: 08.
- Leea SJ, Lo CCH, Matlage PN, Song V, Melikhov Y, Snyder JE, Jiles DC. *J. Appl. Phys.* 2007; **102**: 073910.

37. Melikhov Y, Synder JE, Lo CCH, Matlage PN, Song SH, Dennis KW, Jiles DC. *IEEE Trans. Magn.* 2006; **42**: 2861.
38. Anjaneyulu T, Murthy PN, Rafi VS, Bademiya, John G S. *Physics and Astronomy*, 2013; **14**:37.
39. Peng Y, Wang Z, Liu W, Zhang H, Zuo W, Tang H, Chen F, Wang B. *Dalton Trans.* 2015; **44(28)**:12871-12877.
40. Banerjee S, Gopal J, Muraleedharan P, Tyagi AK, Raj B. *Current Science*, 2006; **90(10)**:1378-1383.